# Surface volume and gravity changes due to significant earthquakes occurred in central Italy from 2009 to 2016.

Federica Riguzzi[1] Hongbo Tan[2] Chongyang Shen[2]

1 Istituto Nazionale di Geofisica e Vulcanologia, Rome, Italy, federica.riguzzi@ingv.it

2 Institute of Seismology, China earthquake Administration, Wuhan 430071, China

## Abstract

We have modelled the surface volume and gravity changes caused by four seismic events: three mainshocks (moment magnitude $M_w$ 6.0, 5.9, 6.5) occurred during the last seismic period started on 2016, August 24 in central Italy, and the 2009, April 6 L'Aquila earthquake ($M_w$ 6.3). Our calculations start from the source parameters estimated by the inversion of the largest dataset of Interferometric Synthetic Aperture Radar (InSAR) and Global Positioning System (GPS) observations ever managed in Italy after earthquake occurrences, based on the half-space elastic dislocation theory. The vertical displacements modelled after the 2016 events allow to infer a substantial unbalance between the subsided and uplifted volumes. In particular, we detected ~106*$10^6$$m^3$ of hangingwall subsidence against ~37*$10^6$$m^3$ of footwall uplift, that accounts for ~74% of the total volume mobilization. From the ratio between the footwall and total deformed volumes, we have computed an average fault dip of ~47º, in line with the values retrieved by seismological methods.

The total gravity variations which affected the study area are of the order of ~1μGal in the far field, and ~170μGal in the near field. The area affected within a gravity change of 1μGal is ~140km long and ~57km wide, parallel to the Apennines mountain chain. The larger

contribution is given by positive variations which account for the tensional style of deformation and larger subsided area.

The significant gravity variations modelled from the coseismic deformations point out the need to update our knowledge about the absolute gravity field in Italy carrying out extensive measurements, and to align Italy to the recent international standards about national gravity and height networks (International Association of Geodesy, IAG report 2015).

## Introduction

An earthquake is an instantaneous frictional sliding along part of the fault area which causes coseismic deformations and mass redistribution; if a gravimeter were located on the Earth surface could measure variations of the local gravity acceleration associated to such sudden event. Static gravity changes have been measured (far field amplitude ~1μGal) by superconducting gravimeters and satellite gravity gradiometers long after the end of the rupture in occasion of large seismic events (e.g., in Japan: 2003, Tokachi-oki $M_w$ 8.0 and 2011, Tohoku $M_w$ 9.0; Imanishi et al. 2004; Cambiotti and Sabadini 2013 and references therein). Recently, transient gravity perturbations produced by earthquakes during the process of fault rupture have been modelled and measured (far field amplitudes of ~$10^{-1}$μGal); such gravity signal reaches a gravimeter located at a certain distance from the source before the arrival of seismic P waves, with amplitude decaying as ~$1/r^2$ (e.g. Harms 2015; Montagner et al. 2016; Vallée et al. 2017), thus opening new light on early warning systems (Juhel et al. 2018). If the same gravimeter were continuously working, could also record postseismic relaxation and redistribution of fluids due to viscoelastic and poroelastic transient phenomena (Van Camp et al. 2017 and references therein). Gravity changes recorded by a

gravimeter consist of two terms: the effect of vertical displacement of Earth's surface and a contribution of internal mass redistribution. Gravity observations alone cannot differentiate between the two. Consequently, the simultaneous and continuous measurement of gravity, through absolute gravimeters, and deformations, through geodetic measurements near epicentral areas, help to separate the competing effects of deformation and mass-fluid redistribution both of tectonic and climatologic origin (Van Camp et al. 2016).

The theory of earthquake sources described by dislocations buried in homogeneous and perfectly elastic isotropic half-space has been from the sixties a great success since able to fit well the observed coseismic deformations (Maruyama 1964; Press 1965; Okada 1985). Okubo (1991, 1992) extended the theory to model the gravity and potential field changes caused by faulting in elastic half-space, showing that the computed gravity changes reveal characteristic patterns similar to those of change in elevation. More recently, viscoelastic and spherical Earth models have also been considered by many scientists (e.g. Pollitz 1996,1997; Wang 1999; Sun 1996, 1998; Wang 2006; Fu 2007). However, the classical elastic dislocation theory works well and is still widely used for easy calculation and good fit with observations (e.g. Toda et al. 2005 and reference therein).

The aim of this work is to model by the classical fault dislocation theory in elastic half-space, the static gravity (e.g. Shen et al. 2010) and surface volume variations due to four significant earthquakes which occurred in recent years in central Italy.

We study the three largest events ($M_w$ 6.0, 5.9, 6.5) of the 2016 seismic sequence and the L'Aquila 2009, 6 April mainshock ($M_w$ 6.3), whose fault sources modelled from space geodetic observations (Cheloni et al. 2017; Cheloni et al. 2014) allow us to depict the spatial patterns and amplitudes of the induced variations.

## Seismotectonic setting

The Apennines are generated by the westerly directed subduction of the Adriatic plate which is characterised by compressional seismicity east of the chain, in the frontal accretionary prism, and extensional tectonics to the west, associated to the opening of the Tyrrhenian backarc basin (e.g. Devoti et al. 2008 and references therein).

The central Appenines are currently affected by SW-NE active extension of 3-4 mm/yr , well evidenced by long term geodetic observations (Devoti et al., 2017), which is accommodated by a systems of NW-SE striking normal faults (Boncio et al. 2004, Brozzetti et al., 2009, Valentini et al. 2019).

In the past, this Apennine sector has been periodically hit by seismic events of moderate magnitude and high intensity. They generated substantial damage to the villages due to poor building masonry, and killed many people, reaching up to X MCS intensity scale (Locati et al. 2016).

On August 24, 2016, at 01:36 (UTC), a $M_w$ 6.0 earthquake struck the study area after a significant seismic quiescence (Gentili et al. 2017). It was the beginning of the most disastrous and long seismic sequence in Italy since 1980 (M 6.9 Irpinia earthquake, southern Apennines). This event destroyed the small villages of Accumoli and Amatrice causing about 300 fatalities, and was followed by a large aftershock sequence with a second relevant event on October 26, $M_w$ 5.9, located about 30 km further north, near Visso. On October 30, the sequence culminated with the largest event, $M_w$ 6.5, with epicenter near Norcia, in the area between the two preceding events (Figure 1), thus filling the gap between the previously activated faults(source parameters and earthquake list at http://terremoti.ingv.it\en). The

struck area is characterized by NW-SE trending normal fault systems, already recognized as tectonically active in the past and often segmented by pre-existing tectonic structures inherited from the pre-Quaternary compressional tectonic phases (Galadini and Galli 2003; Pizzi and Galadini 2009). The 2016 seismic sequence has been ascribed to the reactivation of at least four major normal faults (Figure 1): the Monte Gorzano fault (GF) and the southern part of the Monte Vettore fault (SVF) with the August 24 double event, the Monte Bove fault (BF) with the October 26 event, and the Monte Vettore fault (VF) with the October 30 largest shock (Falcucci et al. 2016; Brozzetti et al. 2019; Iezzi et al. 2019). The area of interest is located between the sector struck in 2009 by the L'Aquila seismic sequence at SE (mainshock on April 6, $M_w$ 6.3; Pondrelli et al. 2010) and the area hit in 1997 by the Colfiorito seismic sequence at NW (Chiaraluce et al. 2004). Figure 1 shows the background seismicity (INGV databank, M≥2.5, depth≤30km), coloured according to the time spans: 1985-2008 (yellow dots), 2009-2016 (blue dots), 2016-2019 (black dots) and events with M>5.0 (red stars). The seismicity of 2016 (black) has filled the gap between the residual seismicity of 1997 Colfiorito (yellow) and the 2009 (blue) seismic sequences (e.g. Ciaccio 2016 and references therein).

Study on the directivity index has clearly confirmed the bilateral rupture of the Amatrice earthquake that nucleated from the hypocenter and propagated in two opposite directions towards S-SE and N-NE (Calderoni et al. 2017; Tinti et al. 2016). The rupture of asperities on either side of nucleation has been well evidenced also by SAR imagery (Lavecchia et al. 2016; Cheloni et al. 2017).

The focal mechanisms estimated from seismology are well in agreement with the tensional tectonic style (Chiaraluce et al. 2017), with planes parallel to the main fault systems. From 24

August 2016 to now (May 2019), the automatic locating procedure resulted in more than 100000 earthquake detections that have been located using the most recent regional velocity model (Chiarabba et al. 2018). The list of preliminary locations and magnitude estimations ($M_L$>0) manually revised by the seismologists of the surveillance service is available at http://terremoti.ingv.it\en.

Moreover, recent papers have evidenced the relevant role played by fluids during the process of earthquake nucleation in central Apennines area, where the fault reactivation and the occurrence of sequences with multiple mainshocks are favoured by the increase of pore pressure at the footwall. The positive Vp/Vs anomaly before the mainshock occurrence has been interpreted as indicator of fluid redistribution at depth (Chiarabba et al. 2018; Malagnini et al. 2012; Di Luccio et al. 2010).

## Geodetic observations and source models

· *The 2016 mainshocks*

The source parameters of the three mainshocks were estimated from a large geodetic data set of both InSAR and GPS measurements, at first processed separately (Cheloni et al. 2017). The InSAR deformation field was retrieved from unwrapped interferograms acquired by different satellites (ALOS-2, Sentinel-1 and COSMO-SkyMed sensors), five across the epoch of Amatrice event, and other three across the epochs of the Visso and Norcia events (Lavecchia et al. 2016). The largest Line of Sight (LoS) displacements detected from InSAR processing were ~-20 cm after the August, 24 event, and ~-90 cm after the October, 30 event. The InSAR data were then down-sampled using a resolution-based resampling technique to perform a lighter joint inversion with GPS data (Cheloni et al., 2017).

The GPS deformation field was obtained after processing data from several continuous and survey mode GPS networks operating in the area (Galvani et al. 2012; Devoti and Riguzzi 2017). The raw GPS observations were processed using the GAMIT/GLOBK, GIPSY and BERNESE software, as described in Devoti et al. (2017), to obtain three distinct time series of daily positions in the International Terrestrial Reference Frame (ITRF2008), for several stations located mostly in the central Mediterranean area. Earthquakes can be detected by a network of GPS stations as step-like offsets on the daily time series of coordinate components (Up, East, North. In our case were obtained three sets of coseismic steps, one for each software solution The final coseismic displacement field has been then obtained by solving for the combined offsets (unknowns) of those coming from the three different solutions, in a least-squares sense (see Devoti 2012). The maxima estimated displacements were subsidence of ~17 cm (after the first event), and from ~20 cm to ~40 cm (after the second and third mainshocks respectively). The horizontal displacements were significant too, evidencing large extension of ~70 cm along the SW-NE direction (Cheloni et al. 2017).

The source modelling is based on the classical theory of rectangular dislocations in an elastic, homogeneous and isotropic half-space (Okada 1985), following a two-step procedure: a nonlinear optimization of fault geometry with assumed uniform slip, then a linear slip distribution inversion on the fault with optimized fixed geometry whose area is composed by patches of increasing size with depth to account for the spatial variability of asperity ruptures. The procedure is described in detail in Cheloni et al. (2017). Both the down-sampled InSAR and GPS datasets were used in the inversions by applying a relative weight to suitably merge their contribution. The best fitting source model of the 24 August earthquake is composed by two rupture areas. The first is the Gorzano fault (GF) and the second the southern Vettore

fault (SVF), both are mainly normal faults with minor left-lateral strike-slip components. On 26 October ruptured the Monte Bove fault (BF) and on 30 October the Vettore fault (VF), both earthquakes are normal. The comprehensive source parameters estimated for the four faults are reported in Table 1.

· *The 2009 L'Aquila earthquake*

The source parameters of the $M_w$ 6.3 L'Aquila event were estimated by the joint inversion of the classical levelling measurements with InSAR (ENVISAT and ALOS) and GPS measurements, which allowed to obtain the coseismic and postseismic slip distributions of the event and to describe in detail the surface displacements (Cheloni et al. 2014). Space geodetic data were obtained after processing ENVISAT frames (Atzori et al. 2009), and from coordinate time series of permanent and non-permanent GPS stations in the near field (Anzidei et al. 2009, Cheloni et al. 2010). The fault dislocation model was retrieved applying a bounded-values least squares algorithm, to impose bounds on the estimated slip and on the nuisance parameters (Cheloni et al. 2014). The comprehensive fault parameters are reported in Table 1.

**Methodology**

A finite rectangular fault buried in a homogeneous half-space is described by its length $L$, the width $W$, the dip angle $\delta$, and the depth from surface to the fault's bottom $d$, as in Figure 2, where the strike slip, dip slip and tensional components of slip vector are $U_1$, $U_2$ and $U_3$. Thus, the gravity change $\Delta g$ on the surface point ($x_1$, $x_2$, $0$) due to instantaneous slip can be expressed as follows (Okubo1992):

$$\Delta g(x_1, x_2) = \{\rho G\cdot[U_1 S_g(\xi,\eta) + U_2 D_g(\xi,\eta) + U_3 T_g(\xi,\eta)] + \Delta\rho G U_3 C_g(\xi,\eta)\}|| - \beta\Delta h(x_1, x_2) \quad (1)$$

Where $G$ is the gravitational constant ($6.67\cdot10^{-11}$ $Nm^2/kg^2$), $\rho$ is the medium density, $\Delta\rho$ is the difference between the density of the medium and the cavity by tensile fracturing, $\beta=0.3086\times10^{-5}\ ms^{-2}$ is the free-air gravity gradient, $\Delta h(x_1, x_2)$ is the surface elevation change given by

$$\Delta h(x_1, x_2) = \frac{1}{2\pi}[U_1 S_h(\xi,\eta) + U_2 D_h(\xi,\eta) + U_3 T_h(\xi,\eta)]|| \quad (2)$$

where the notation mark || denotes the abbreviation of the following relationship, as suggested by Chinnery (1961)

$$f(\xi,\eta)|| = f(x_1, p) - f(x_1, p-W) - f(x_1-L, p) + f(x_1-L, p-W)$$

Where $p = x_2 cos\delta + dsin\delta$, and $S_g(\xi,\eta)$, $D_g(\xi,\eta)$, $T_g(\xi,\eta)$ and $C_g(\xi,\eta)$ are (Okada 1985) :

$$S_g(\xi,\eta) = -\frac{qsin\delta}{R} + \frac{q^2 cos\delta}{R(R+\eta)}$$

$$D_g(\xi,\eta) = 2I_2 \sin\delta - \frac{q\bar{d}}{R(R+\xi)}$$

$$T_g(\xi,\eta) = 2I_2 \cos\delta + \frac{q\bar{y}}{R(R+\xi)} + \frac{q\xi cos\delta}{R(R+\eta)}$$

$$C_g(\xi,\eta) = 2I_2 \cos\delta - sin\delta \cdot \log(R+\xi)$$

where $\bar{y} = \eta\cos\delta + qsin\delta, \bar{d} = \eta\sin\delta - qcos\delta, q = x_2 sin\delta - dcos\delta, R = \sqrt{\xi^2+\eta^2+q^2}$

||and $S_h, D_h\, T_h$ are

$$S_h(\xi,\eta) = -\frac{q\bar{d}}{R(R+\eta)} - \frac{qsin\delta}{R+\eta} - I_4 sin\delta$$

$$D_h(\xi,\eta) = -\frac{q\bar{d}}{R(R+\xi)} - sin\delta \cdot \tan^{-1}\left(\frac{\xi\eta}{qR}\right) + I_5 sin\delta \cdot cos\delta$$

$$T_h(\xi,\eta) = \frac{q\bar{y}}{R(R+\xi)} + cos\delta \cdot \left[\frac{\xi q}{R(R+\eta)} - \tan^{-1}\left(\frac{\xi\eta}{qR}\right)\right] - I_5 sin^2\delta$$

and

$$I_0(\xi,\eta) = \log(R+\eta) - sin\delta \cdot \log(R+\bar{d})$$

$$I_1(\xi,\eta) = tan^{-1}\left(\frac{-qcos\delta + (1+sin\delta)(R+\eta)}{\xi cos\delta}\right)$$

$$I_2(\xi,\eta) = \tan^{-1}\left(\frac{R+\xi+\eta}{q}\right)$$

$$I_3(\xi,\eta) = (\xi I_0 + 2qI_1)sec^2\delta$$

$$I_4(\xi,\eta) = (1-2v)[\log(R+\bar{d}) - sin\delta \cdot \log(R+\eta)]sec\delta$$

$$I_5(\xi,\eta) = 2(1-2v)I_1 sec\delta$$

**Volume mobilization and gravity changes**

Based on the previous formulation, the individual and joint vertical displacements $\Delta h(x_1, x_2)$ and coseismic gravity changes $\Delta g(x_1, x_2)$ caused by the 2016 Amatrice $M_w$ 6.0, Visso $M_w$ 5.9, Norcia $M_w$ 6.5 and 2009 L'Aquila $M_w$ 6.3 earthquakes are simulated. Taking into account the dimension of the coseismic faulting, we have chosen a grid cell size of 0.01°×0.01° (~1×1km). Figure 3a shows the combined coseismic vertical displacements ($\Delta h$) obtained applying the relationship (2) and the coseismic vertical displacements measured by GPS. The background colour palette represents the surface interpolating the gridded values, with uplift in red and collapse in blue . The interpolation has the effect to smooth the extreme values of $\Delta h$, which indeed range between -80 cm and +6 cm near the Norcia area, and -30 cm and 10 cm near L'Aquila. As already recognized in Cheloni et al. (2017), the single source model of the Norcia earthquake does not reproduce completely the observed displacements (blue arrows, Figure

3a) which are larger than the predicted ones (yellow arrows, Figure 3a), suggesting an interesting tectonic complexity of the area or a lower adequacy of the classical elastic model to this rupture. The peculiar pattern of deformation can be better reproduced by introducing in the modeling ancillary and antithetic sources, or additional gravitational deformations (e.g. Cheloni et al. 2017, Valerio et al. 2018 and references therein). On the contrary, the fine agreement between the predicted and observed displacements of the L'Aquila event evidences a simpler source geometry that fits well with the elastic model (Figure 3a).

Figure 3b shows the topography and the vertical displacements projected along the profile of Figure 3a crossing the source of $M_w$ 6.5 (Norcia mainshock): the transition between the maximum collapsed area and the uplifted sector occurs where the mean topography of the accretionary prism of Apennines subduction is higher.

The gridded vertical displacement of the Amatrice and Norcia events allowed us to compute the subsided and uplifted volumes applying the cut and fill algorithm with respect to the isoline of zero variation (Global Mapper © GIS sw). We infer a substantial unbalance between the subsided and uplifted volumes. In particular, we obtain ~$37\times10^6 m^3$ of footwall uplift and ~$106\times10^6 m^3$ of hangingwall subsidence. The total terrain volume deformed by the earthquakes, computed with respect to the pre-event topographic surface, is ~143 millions of cubic meters, of which ~74% accounts for hangingwall subsidence and the remaining 26% is due to the footwall uplift. In other words, the hangingwall collapsed volume is about 3 times the footwall uplifted one. As expected by elastic dislocation theory (e.g. Segall 2010), the ratio of absolute coseismic displacements of the hangingwall and footwall of a fault that reaches the surface depends on the dip angle and can be easily described by $\delta = \pi \cdot u_f/(u_h+u_f)$, where $\delta$ is the fault dip, $u_f$ and $u_h$ are respectively the footwall and hangingwall displacements (Walsh

1969). It is interesting to note that the same ratio holds also for the mobilized volumes. In fact, applying the formula to the dislocated volumes of Amatrice and Norcia events, the dip angle computed from the ratio $\delta=\pi \cdot V_f/(V_h+V_f)$ , where $V_f$ and $V_h$ are respectively the footwall and hangingwall dislocated volumes, results ~47º. Similar value has been obtained from the focal mechanism of the Norcia main event (INGV databank).

The patterns of vertical displacements and gravity changes are similar but with opposite signs since there is negative relationship between them. The coseismic gravity changes are obtained applying the relationship (1), once known (2).

Figure 4 shows separately the gravity changes of the $M_w$ 6.5 Norcia and the $M_w$ 6.3 L'Aquila mainshocks. Regarding the Norcia event ($M_w$ 6.5 earthquake), our model shows variations from 20 to 160 μGal in the collapsed hangingwall area, and about -10 μGal in the footwall. About the L'Aquila event (Figure 4b), in the near field the changes concentrate mainly around the fault trace, they range between 10 to 45 μGal (1μGal =$10^{-8}ms^{-2}$) in the hangingwall, and reach the maximum value of -4 μGal in the footwall. The change patterns also show a four-quadrant distribution with negative sectors in the northwest and southeast, while positive sectors can be found in the northeast and southwest. The gravity change field decays quickly, with variations in the far field of the order of 1 μGal, therefore below the mean accuracy of any absolute gravimeter.

Finally, Figure 5 shows the combined effects of the four earthquakes in terms of gravity change that is computed as the sum of each one. The focal mechanism solutions of the four earthquakes are similar and indicate that the rupture focuses on normal slip faults. In the near field, gravity increases in the collapsed hangingwall, while it decreases in the footwall. The coseismic gravity changes that can be detected by an absolute gravimeter like FG-5, with

measurement accuracy of 2-5 μGal (Van Camp et al. 2017), are focussed on the two sides of fault zone within ±15km.

## Discussion and Conclusions

The recent and long lasting seismic sequence, started in central Apennines area with the Amatrice event (August, 24 2016), has modified the gravity field of an area as large as ~$4x10^3$ $km^2$. Following the tectonic style of the area and the extensional focal mechanisms of the events, the model evidences a large area of gravity increase, due to the main component of vertical collapse. The modelled vertical displacements due to the 2016 mainshocks allow to infer a substantial unbalance between the subsided and uplifted volumes. In particular, we detected ~$106*10^6 m^3$ of footwall subsidence against ~$37*10^6 m^3$ of hangingwall uplift, that accounts for ~74% of the total volume mobilization. From the ratio between the footwall and total deformed volumes, we have computed an average fault dip of ~47º, in line with the values retrieved by seismological methods.

The gravity changes are computed both individually and composing the vertical displacement fields of the four events. In addition, we have modelled the gravity variation induced by the 2009, April 6 L'Aquila event which was also of extensional style, and the total gravity field variations due to all the considered seismic events. The calculation of the coseismic gravity changes is based on the fault dislocation theory in elastic half-space, starting from the simplest source models retrieved by inverting geodetic observations (Cheloni et al. 2017; Cheloni et al. 2014). From the source models, we have computed the displacements and gravity changes on a regular grid (0.01°x0.01°) both individually and as combined contribution of all the events. The total gravity variations which affected the area are in the order of

~1μGal (~$10^{-8}$ms$^{-2}$) in the far field, and ~170μGal in the near field. The area affected within a gravity change of 1μGal is ~140km long and ~57km wide, parallel to the Apennines chain with a larger contribution due to positive variations, accounting for the tensional style of deformation and larger subsided area. In the hypothesis of carrying out measurements with a classical absolute gravimeter with an accuracy of about 2μGal, the area where significant and measurable variations would be detected is ~110km long and ~40km wide.

Unfortunately, we do not have gravimetric measures available in the central Apennines area neither continuous nor sporadic, so that the Global Navigation Satellite Systems (GNSS) and gravity observations cannot be integrated to separate the effect of density and fluid dependence during the seismic cycle.

The absolute gravity measurements carried out on a framework of a few fundamental stations in Italy date back to 1955 and 1977 (Cunietti and Inghilleri 1955; Marson and Morelli 1977). Up to 2009, at least other 24 seismic events with M≥5.5 occurred in Italy (Rovida et al. 2016) thus modifying significantly the gravity field along the Apennines belt and in NE Alpine sector. Taking into account that we have here neglected many other phenomena that contribute to change permanently the gravity field, like subsidence affecting the Po plain and volcanic activity; all such considerations strongly support the need to plan and conduct extensive and periodical gravity measurements in the Italian area by realizing a new first order absolute gravity network to which to connect aerogravimetric and terrestrial gravity surveys

Acknowledgements

This study is based on geodetic data and models acquired and processed during the 2016 and 2009 earthquake emergencies, therefore we are very grateful to Daniele Cheloni and all

the INGV geodetic team, together we worked intensely and with passion during all that time. We are also grateful to the Reviewers and the Editor, their suggestions helped us to improve the manuscript.

## References

Anzidei M. et al. (2009) Coseismic deformation of the destructive April 6, 2009 L'Aquila earthquake (central Italy) from GPS data. Geophys. Res. Lett. 36 L17307 doi: 10.1029/2009GL039145.

Atzori S., I. Hunstad, M. Chini, S. Salvi, C. Tolomei, C. Bignami,S. Stramondo, E. Trasatti, A. Antonioli and E. Boschi (2009) Finite fault inversion of DInSAR coseismic displacement of the 2009 L'Aquila earthquake (central Italy). Geophys. Res. Lett. 36 L15305 doi: 10.1029/2009GL039293.

Boncio P., Lavecchia G., Pace B. (2004) Defining a model of 3D seismogenic sources for Seismic Hazard Assessmentapplications: The case of central Apennines (Italy). J. Seismology 8 407-425.

Brozzetti F., Boncio P., Lavecchia G., Pace B. (2009) Present activity and seismogenic potential of a low-angle normal fault system (Città di Castello, Italy): Constraints from surface geology, seismic reflection data and seismicity. Tectonophysics 463 31-46 doi:10.1016/j.tecto.2008.09.023.

Calderoni G., Rovelli A., & Di Giovambattista R. (2017) Rupture directivity of the strongest 2016–2017 central Italy earthquakes. J. Geophys. Res. Solid Earth 122 9118–9131 doi: 10.1002/2017JB014118.

Cambiotti G., Sabadini R. (2013) Gravitational seismology retrieving Centroid-Moment-Tensor solution of the 2011 Tohoku earthquake. J. Geophys. Res. Solid Earth 118 183–194 doi: 10.1029/2012JB009555.

Cheloni D., D'Agostino N., D'Anastasio E., Avallone A., Mantenuto S., Giuliani R., Mattone M., Calcaterra S., Gambino P., Dominici D., Radicioni F., Castellini F., (2010) Coseismic and initial postseismic slip of the 2009 $M_W$ 6.3 L'Aquila earthquake, Italy, from GPS measurements. Geophys. J. Int. 181 1539–1546 doi: 10.1111/j.1365-246X.2010.04584.x.

Cheloni D., Giuliani R., D'Anastasio E., Atzori S., Walters R.J., Bonc, L., D'Agostino N., Mattone M., Calcaterra S., Gambino P., Deninno F., Maseroli R., Stefanelli G. (2014) Coseismic and post-seismic slip of the 2009 L'Aquila (central Italy) $M_W$ 6.3 earthquake and implications for seismic potential along the Campotosto fault from joint inversion of high-precision levelling, InSAR and GPS data. Tectonophysics 622 168–185 doi: 10.1016/j.tecto.2014.03.009.

Cheloni D., et al. (2017) Geodetic model of the 2016 Central Italy earthquake sequence inferred from InSAR and GPS data. Geophys. Res. Lett. 44 6778–6787 doi: 10.1002/2017GL073580.

Chiarabba C., De Gori P., Cattaneo M., Spallarossa D., Segou M. (2018) Faults geometry and the role of fluids in the 2016–2017 Central Italy seismic sequence. Geophys. Res. Lett. 45 6963–6971 doi: 10.1029/2018GL077485.

Chiaraluce L., Amato A., Cocco M., Chiarabba C., Selvaggi G., Di Bona M., Piccinini D., Deschamps A., Margheriti L., Courboulex F., Ripepe M. (2004) Complex normal faulting in the Apenninesthrust-and-fold belt: The 1997 seismic sequence in central Italy. Bull.Seismol. Soc. Am. 94(1) 99–116.

Chiaraluce L., Di Stefano R., Tinti E., Scognamiglio L., Michele M., Casarotti M., Cattaneo M., De Gori, P., Chiarabba C. et al. (2017) The 2016 Central Italy Seismic Sequence: A First Look at the Mainshocks, Aftershocks, and Source Models. Seismol. Res. Lett. 88 757–771.

Chinnery M.A.(1961) The deformation of ground around surface faults. Bull. Seism. Soc. Am. 51 355-372.

Ciaccio M.G. (2016) Instrumental seismicity of the Amatrice earthquake epicentral area: a review. Ann. Geophys. 59 Fast Track 5 doi: 10.4401/ag-7283.

Cunietti M., Inghilleri E. (1955) La rete gravimetrica fondamentale italiana. Memorie Commissione Geodetica Italiana 8 192 pp, in Italian.

Devoti R., Riguzzi F., Cuffaro M., Doglioni C. (2008) New GPS constraints on thekinematics of the Apennines subduction. Earth Planet. Sci. Lett. 273 163–174.

Devoti R. (2012) Combination of coseismic displacement fields: a geodetic perspective. Ann. Geophys. 55 4 781-787 doi: 10.4401/ag-6119.

Devoti R., N. D'Agostino, E. Serpelloni, G. Pietrantonio, F. Riguzzi, A. Avallone, A. Cavaliere, D. Cheloni, G. Cecere, C. D'Ambrosio, L. Falco, G. Selvaggi, M. Métois, A. Esposito, V. Sepe, A. Galvani, and M. Anzidei (2017) The Mediterranean Crustal Motion Map compiled at INGV. Ann. Geophys. 60 (2) doi: 10.4401/ag-7059.

Devoti R., Riguzzi F. (2017) The velocity field of the Italian area. Rend. Fis. Acc. Lincei 29 (Suppl 1) S51-S58 doi: 10.1007/s12210-017-0651-x.

Di Luccio F., Ventura G., Di Giovambattista R., Piscini A., Cinti F. R. (2010) Normal faults and thrusts reactivated by deep fluids: The 6 April 2009 $M_w$ 6.3 L'Aquila earthquake, central Italy. J. Geophys. Res. 115 B06315 doi: 10.1029/2009JB007190

Falcucci E., S. Gori, E. Peronace, G. Fubelli, M. Moro, M. Saroli, B. Giaccio, P. Messina, G. Naso, G. Scardia, A. Sposato, M. Voltaggio, P. Galli, F. Galadini (2009) The Paganica fault and surface coseismic ruptures caused by the 6 April 2009 earthquake (L'Aquila, central Italy). Seism. Res. Lett. 80 (6) 940-950.

Falcucci E., Gori S., Galadini F., Fubelli G., Moro M., Saroli M. (2016) Active faults in the epicentral and mesoseismal Ml 6.0 24, 2016 Amatrice earthquake region, central Italy. Methodological and seismotectonic issues. Ann. Geophys. 59 Fast Track 5 doi: 10.4401/ag-7266.

Fu G. (2007) Surface Gravity Changes Caused by Tied-Generating Potential and by Inernal Dislocation in a 3-D Heterogeneous Earth. Thesis, Univ. of Tokyo, Japan.

Galadini F., Galli P. (2003) Paleoseismology of silent faults in the Central Apennines (Italy): the Mt. Vettore and Laga Mts. Faults. Ann. Geophys 46 5 815-836 doi: 10.4401/ag-3457

Galvani A., M. Anzidei, R. Devoti, A. Esposito, G. Pietrantonio, A.R. Pisani, F. Riguzzi, and E. Serpelloni (2012) The interseismic velocity field of the central Apennines from a dense GPS network. Ann. Geophys. 55 (4) doi: 10.4401/ag-6168.

Gentili S., Di Giovambattista, R., Peresan A. (2017) Seismic quiescence preceding the central Italy earthquakes. PEPI 272 27-33 doi: 10.1016/j.pepi.2017.09.004

Harms J., Ampuero J.-P., Barsuglia M., Chassande-Mottin E., Montagner J.-P., Somala S.N. & Whiting B.F. (2015) Transient gravity perturbations induced by earthquake rupture, Geophys. J. Int. **201**(3) 1416–1425.

IAG report (2015) Commission 2 – Gravity Field http://www.iag-commission2.ch

Iezzi F., Roberts G., Faure Walker J., Papanikolaou I. (2019) Occurrence of partial and total coseismic ruptures of segmented normal fault systems: Insights from the Central Apennines, Italy. J. Structural Geology 126 83-99 doi: 10.1016/j.jsg.2019.05.003

Imanishi Y., Sato T., Higashi T., Sun W., Okubo S. (2004) A network of superconducting gravimeters detects submicrogal coseismic gravity changes. Science 306 476–478.

Juhel K., Ampuero J.-P., Barsuglia M., Bernard P., Chassande-Mottin E., Fiorucci D., et al. (2018) Earthquake early warning using future generation gravity strainmeters. J. Geophys. Res. Solid Earth 123 doi: 10.1029/2018JB016698

Lavecchia G. et al. (2016) Ground deformation and source geometry of the 24 August 2016 Amatrice earth- quake (Central Italy) investigated through analytical and numerical modeling of DInSAR measurements and structural-geological data. Geophys. Res. Lett. 43 12,389–12398 doi: 10.1002/2016GL071723.

Locati M., Camassi R., Rovida A., Ercolani E., Bernardini F., Castelli V., Caracciolo C.H., Tertulliani A., Rossi A., Azzaro R., D'Amico S., Conte S., Rocchetti E. (2016) DBMI15, the 2015 version of the Italian Macroseismic Database. Istituto Nazionale di Geofisica e Vulcanologia doi: 10.6092/INGV.IT-DBMI15.

Malagnini L., Lucente F.P., De Gori P., Akinci A., Munafo I. (2012) Control of pore fluid pressure diffusion on fault failure mode: Insightsfrom the 2009 L'Aquila seismic sequence. J. Geophys. Res. 117 B05302 doi: 10.1029/2011JB008911

Marson I., Morelli C. (1977) First Order Gravity Net in Italy. Bollettino di Geodesia e Scienze Affini XXXVII 4 659-689.

Maruyama T. (1964) Static elastic dislocations In an infinite and semi- infinite medium. Bull. Earthq. Res. Inst. Tokyo university 42 289-368.

Montagner J.-P., Juhel K., Barsuglia M., Ampuero J.P., Chassande-Mottin E., Harms J., Whiting B., Bernard P., Clévédé E., Lognonné P. (2016) Prompt gravity signal induced by the 2011 Tohoku-Oki earthquake. Nature Communications 7 13349 doi:10.1038/ncomms13349

Okada Y. (1985) Surface deformation due to shear and tensile faults in a half-space. Bull. Seismol. Soc. Am. 75 1135–1154.

Okubo S. (1991) Potential and gravity changes raised by point dislocations. Geophys. J. Int. 105 573-586.

Okubo S. (1992) Gravity and potential changes due to shear and tensile faults in a half-space. J. Geophys. Res. 97 7137-7144.

Pizzi A., Galadini F. (2009) Pre-existing cross-structures and active fault segmentation in the northern-central Apennines (Italy). Tectonophysics 476 1-2 304-319 doi: 10.1016/j.tecto.2009.03.018.

Press F. (1965) Displacements, strains, and tilts at teleseismic distances. J. Geophys. Res. 70 2395-2412.

Pollitz F.F. (1996) Coseismic deformation from earthquake faulting in a layered spherical Earth. Geophys. J. Int. 125 1-4.

Pollitz F.F. (1997) Gravitational viscoelastic postseismic relaxation on a layered spherical Earth. J. Geophys. Res. 102(B8) 17921-17941.

Pondrelli S., Salimbeni S., Morelli A., Ekström G., Olivieri M., Boschi E. (2010) Seismic moment tensors of the April 2009, L'Aquila (Central Italy), earthquake sequence. Geophys. J. Int. 180 1 238–242 doi: 10.1111/j.1365-246X.2009.04418.x

Rovida A., Locati M., Camassi R., Lolli B., Gasperini P. (eds) (2016) CPTI15, the 2015 version of the Parametric Catalogue of Italian Earthquakes. Istituto Nazionale di Geofisica e Vulcanologia doi: 10.6092/INGV.IT-CPTI15.

Segall P. (2010) Earthquake and Volcano Deformations, Princeton University Press.

Shen C., Li H., Tan H. (2010) Simulation of co-seismic gravity change and deformation of Wenchuan Ms 8.0 earthquake. Geodesy and Geodynamics 1 1-14 doi: 10.3724/SP.J.1246.2010.00008.

Sun W., Okubo S., Vanicek P. (1996) Global displacement caused by dislocations in a realistic Earth model. J. Geophys. Res. 101 8561-8577.

Sun W., Okubo S. (1998) Surface potential and gravity changes due to internal dislocations in a spherical Earth II. Application to a finite fault. Geophys. J. Int. 132 79-88.

Tinti E., Scognamiglio L., Michelini A., Cocco M. (2016) Slip heterogeneity and directivity of the ML 6.0, 2016, Amatrice earthquake estimated with rapid finite-fault inversion. Geophys. Res. Lett. 43 10745–10752 doi: 10.1002/2016GL071263.

Toda S., Stein R.S., Richards-Dinger K., Bozkurt S. (2005) Forecasting the evolution of seismicity in southern California: Animation built on earthquake stress transfer. J. Geophys. Res. 110 B05S16 doi:10.1029/2004JB003415.

Valentini A., Pace B., Boncio P., Visini F., Pagliaroli A., Pergalani F. (2019) Definition of seismic input from fault‐based PSHA:Remarks after the 2016 central Italy earthquake sequence.Tectonics 38 doi:10.1029/2018TC005086

Valerio E., Tizzani P., Carminati E., Doglioni C., Pepe S., Petricca P., De Luca C., Bignami C., Solaro G., Castaldo R., De Novellis V., Lanari R. (2018) Ground Deformation and Source Geometry of the 30 October 2016 $M_w$ 6.5 Norcia Earthquake (Central Italy)

Investigated Through Seismological Data, DInSAR Measurements, and Numerical Modelling. Remote Sensing 10 1901 doi:10.3390/rs10121901.

Vallée M., Ampuero J.P., Juhel K., Bernard P., Montagner J.P., Barsuglia M. (2017) Observations and modeling of the elastogravity signals preceding direct seismic waves. Science 358 (6367) 1164-1168.

Van Camp M., de Viron O., Avouac J.-P. (2016) Separating climate-induced mass transfers and instrumental effects from tectonic signal in repeated absolute gravity measurements. Geophys. Res. Lett. 43 4313–4320 doi:10.1002/2016GL068648.

Van Camp M., de Viron O., Watlet A., Meurers B., Francis O., Caudron C. (2017) Geophysics from terrestrial time-variable gravity measurements. Reviews of Geophysics 55 938-992 doi:10.1002/2017rg000566

Walsh J.B. (1969) Dip angle of faults as calculated from surface deformation. J. Geophys. Res. 74 8 2070-2080.

Wang H. (1999) Surface vertical displacements potential, perturbations and gravity changes of a viscoelastic Earth model induced by internal point dislocations. Geophys. J. Int. 137(2) 429-440.

Wang R., Lorenzo-Martin F., Roth F. (2006) PSGRN/PSCMP- a new code for calculation co- and post-seismic deformation, geoid and gravity changes based on the viscoelastic-gravitational dislocation theory. Computers and Geosciences 32 527-541.

**Figure captions**

**Figure1**: Map of the study area. Source models of the October 30 (red box), August 24, October 26 and April 6 2009 events (blue boxes) as retrieved after the inversion of geodetic observations, projected on the topographic surface. The epicentres (red stars $5.0<M_w\leq6.5$ ) and focal mechanisms of the mainshocks (beach balls, $M_w\geq5.9$) are shown. Some major active faults are drawn (black lines: BF=Bove fault, VF=Vettore fault; SVF= Southern VF; GF= Gorzano fault; PF= Paganica Fault). Background seismicity from INGV databank (M≥2.5, max depth 30km): 01/01/1985-31/12/2008 (yellow dots); 01/01/2009-23/08/2016 (blue dots); 24/08/2016-03/01/2019 (black dots)

**Figure 2**: Classical dislocation model of a rectangular fault (Okada, 1985): each vector represents the displacement component of the hangingwall side block relative to the footwall in the fault reference system. In the figure, $U_2>0$ denotes a thrust fault-type motion, while $U_2<0$ denotes a normal fault fault-type movement.

**Figure 3**: a) Pattern of the coseismic vertical displacements obtained from the source models of i) April, 6 2009 L'Aquila earthquake (Cheloni et al., 2014); ii) August, 24 2016 Amatrice event and iii) October, 26 and 30 2016 Visso and Norcia events (Cheloni et al., 2017); the blue arrows are the vertical coseismic offsets detected by GPS and the yellow arrows are the offsets predicted by the source models. A-A' is the section shown in b)

b) profile (A-A') across the source of $M_w$ 6.5 Norcia earthquake, the topography in gray, the vertical displacements in blue and the red dashed line is the fault plane along the profile. Uplift and collapse are indicated respectively by red and blue arrows.

**Figure 4**: Coseismic gravity changes obtained from each source model of the two main-shocks of a) Norcia (October 30 2016) , b) L'Aquila (April 6 2009). In blue are indicated the areas of negative gravity variation (uplift), from green to red colours the positive variations (collapse).

**Figure 5**: Coseismic gravity changes modelled for all the earthquakes. In blue are indicated the areas of negative gravity variation (uplift), from green to red colours the positive variations (collapse).

Table 1: Fault models of 2016 and 2009 mainshocks from geodetic data

| Seismic Event | Size (km×km) | Patches # | Peak slip (m) | Strike (deg) | Dip (deg) | Seismic Moment ($\times 10^{18}$ Nm) | Mw |
|---|---|---|---|---|---|---|---|
| 24 Aug. 2016 GF | 14×14 | 532 | 0.89 | 163.6 | 52 | 2.1 | 6.2 |
| 24 Aug. 2016 SVF | 10×10 | 420 | 1.40 | 168.5 | 41 | | |
| 26 Oct. 2016 BF | 20×16.5 | 94 | 0.70 | 158 | 43 | 2.0 | 6.2 |
| 30 Oct. 2016 VF | 20×19.5 | 134 | 2.22 | 158 | 43 | 8.5 | 6.6 |
| 6 Apr. 2009 | 28×20.8 | 135 | 0.77 | 140 | 50 | 3.8 | 6.3 |

Figure



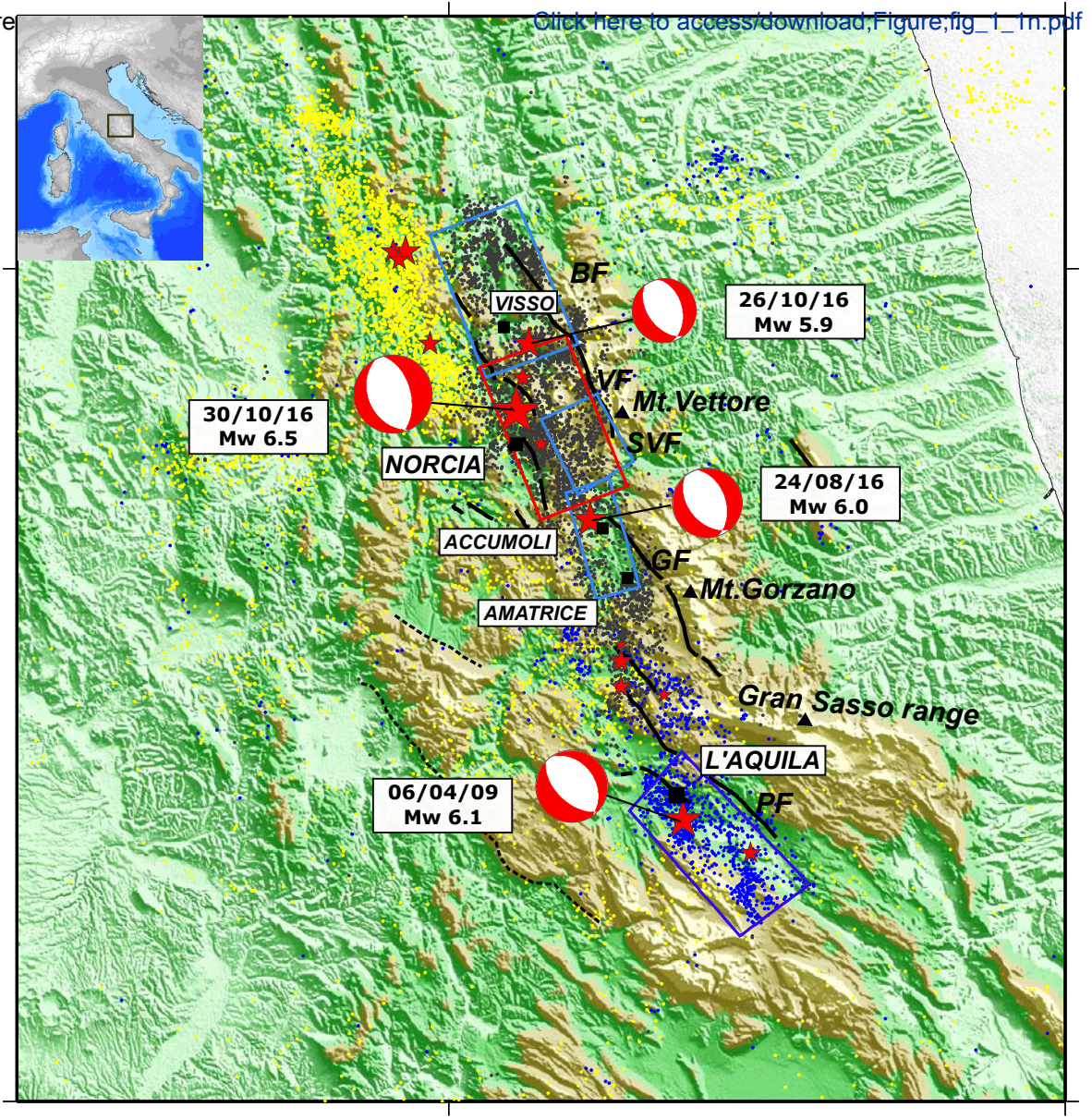

Figure

Click here to access/download;Figure;fig_2_fault_

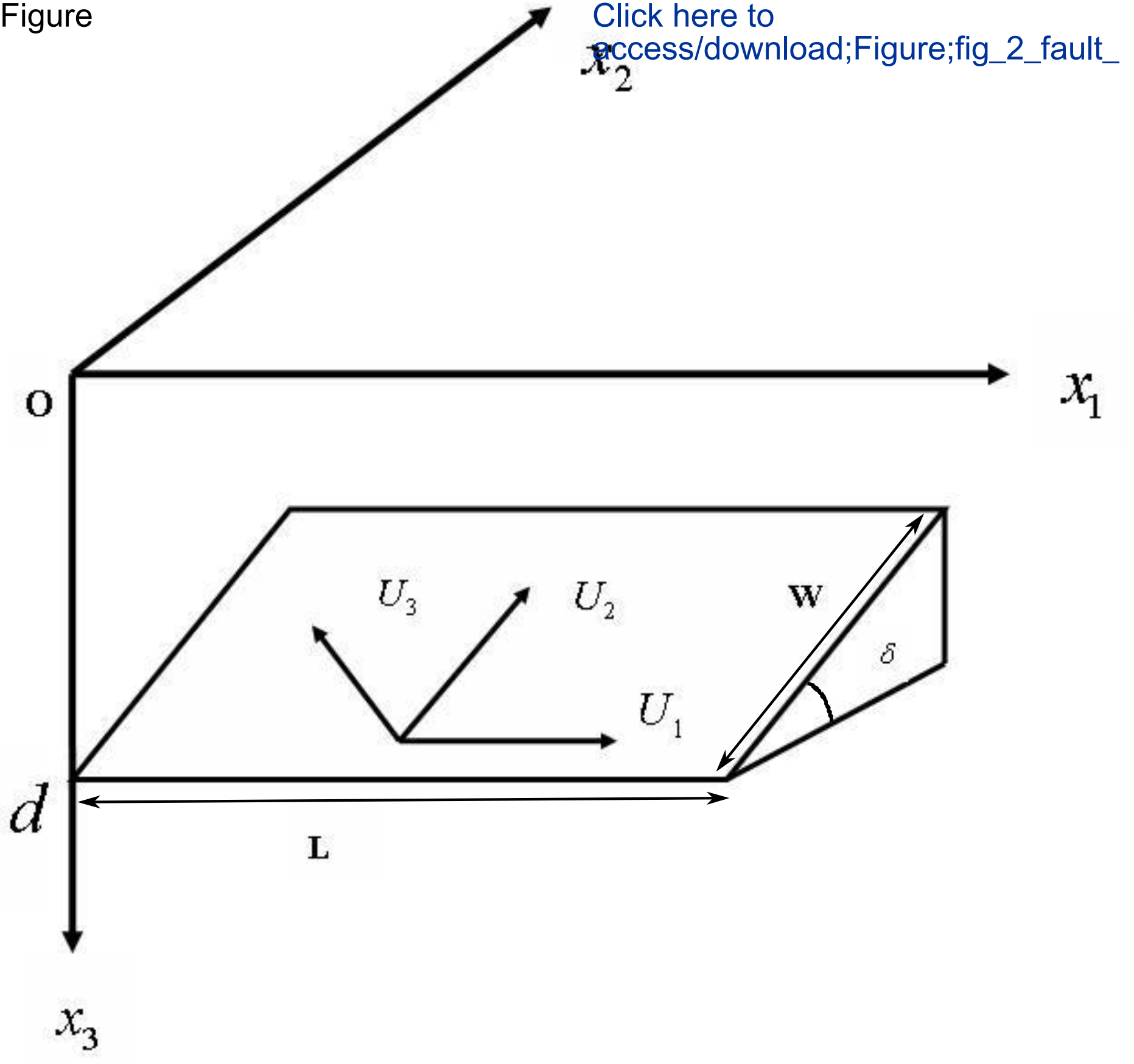

Figure

Click here to access/download;Figure;fig_3a_dh_new.pdf

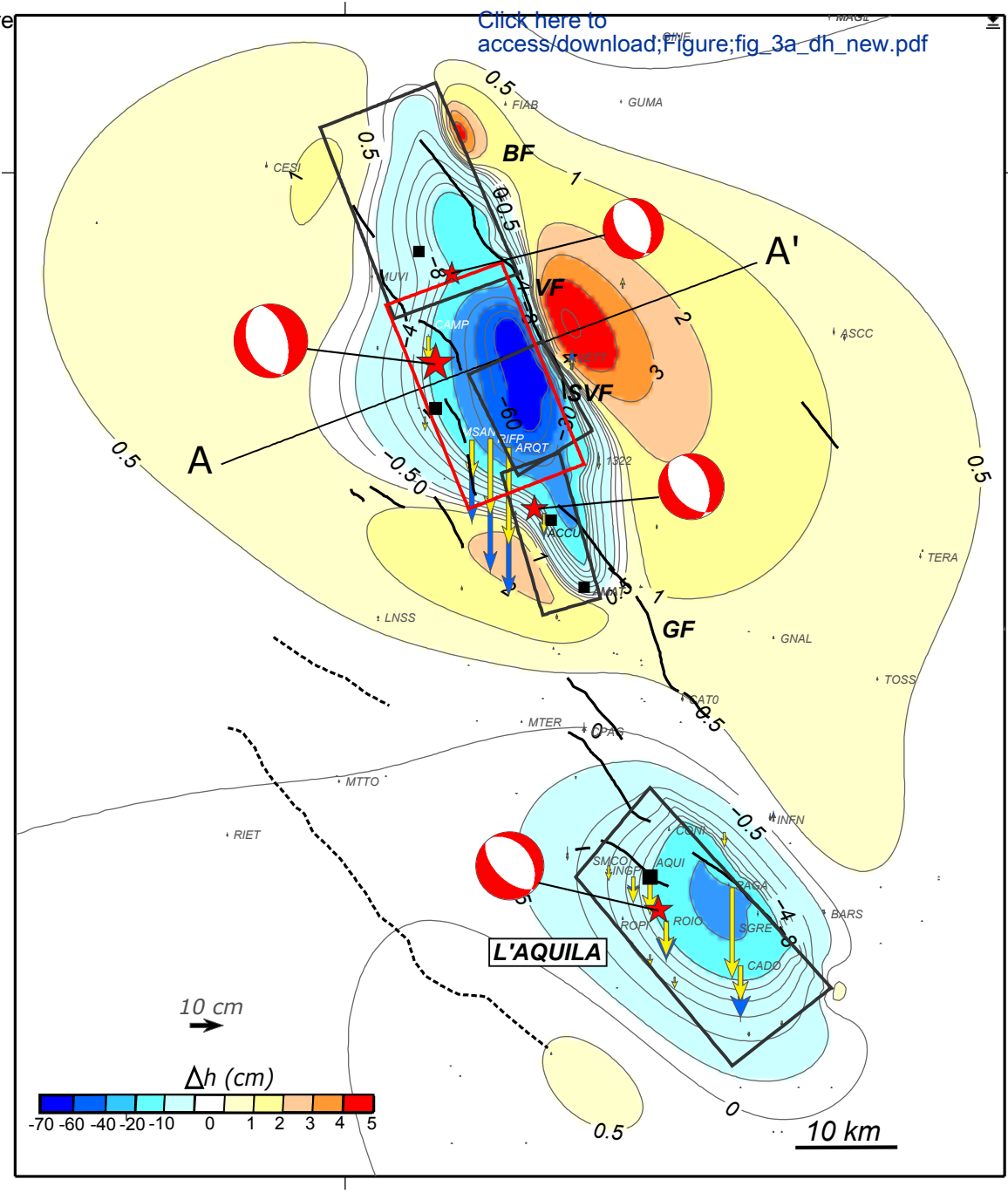

Figure

Click here to access/download;Figure;fig_3b_profilo_new_dh.pdf

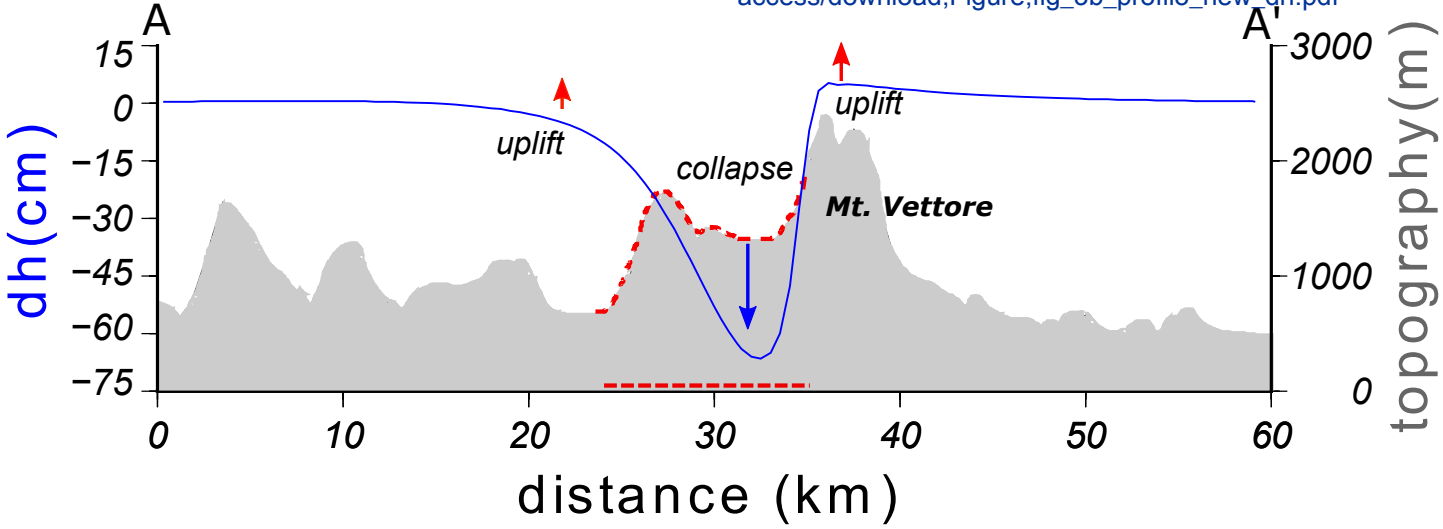

Figure

Click here to access/download;Figure;fig_4_30oct_plus.pdf

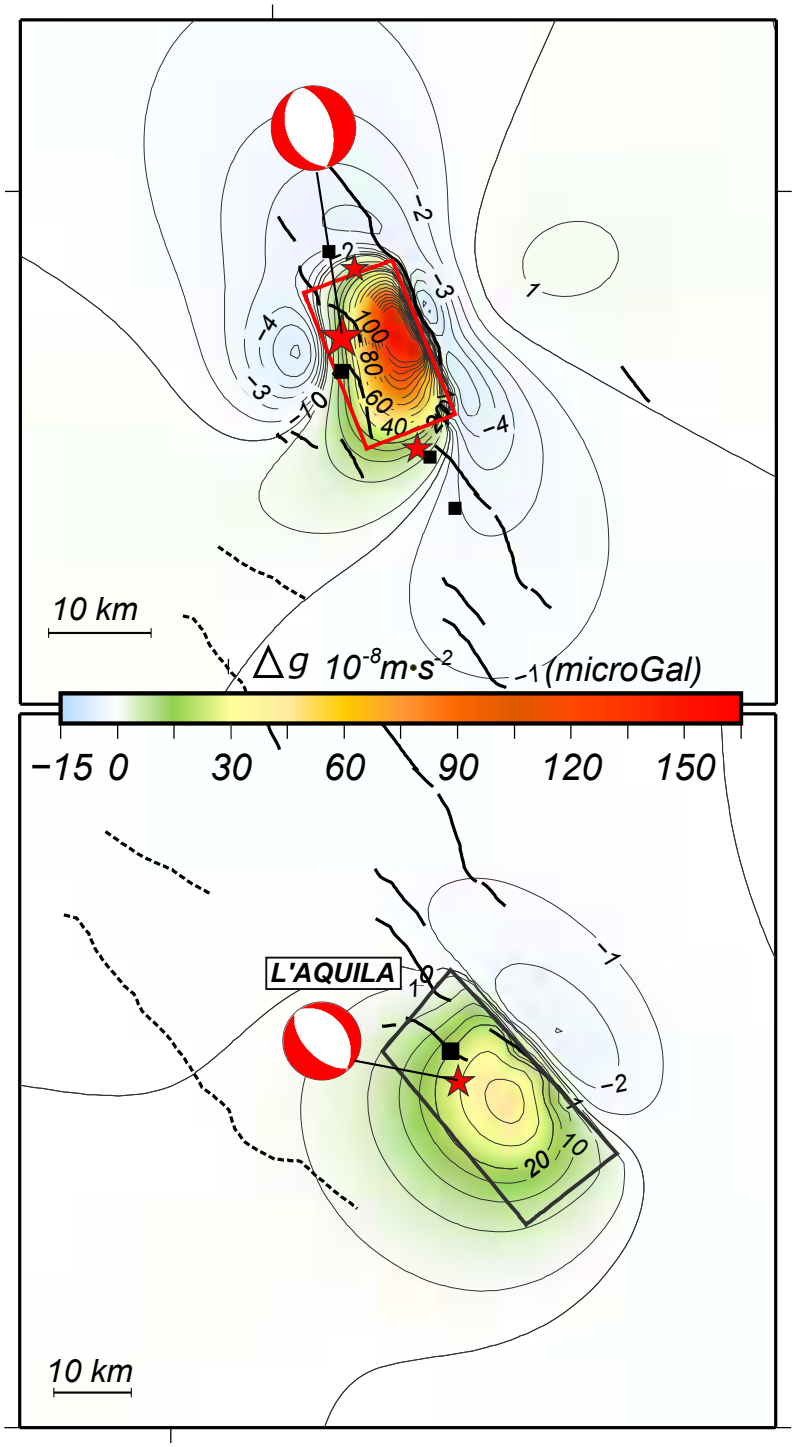

Figure

Click here to access/download;Figure;fig_5_grav_23apr.pdf

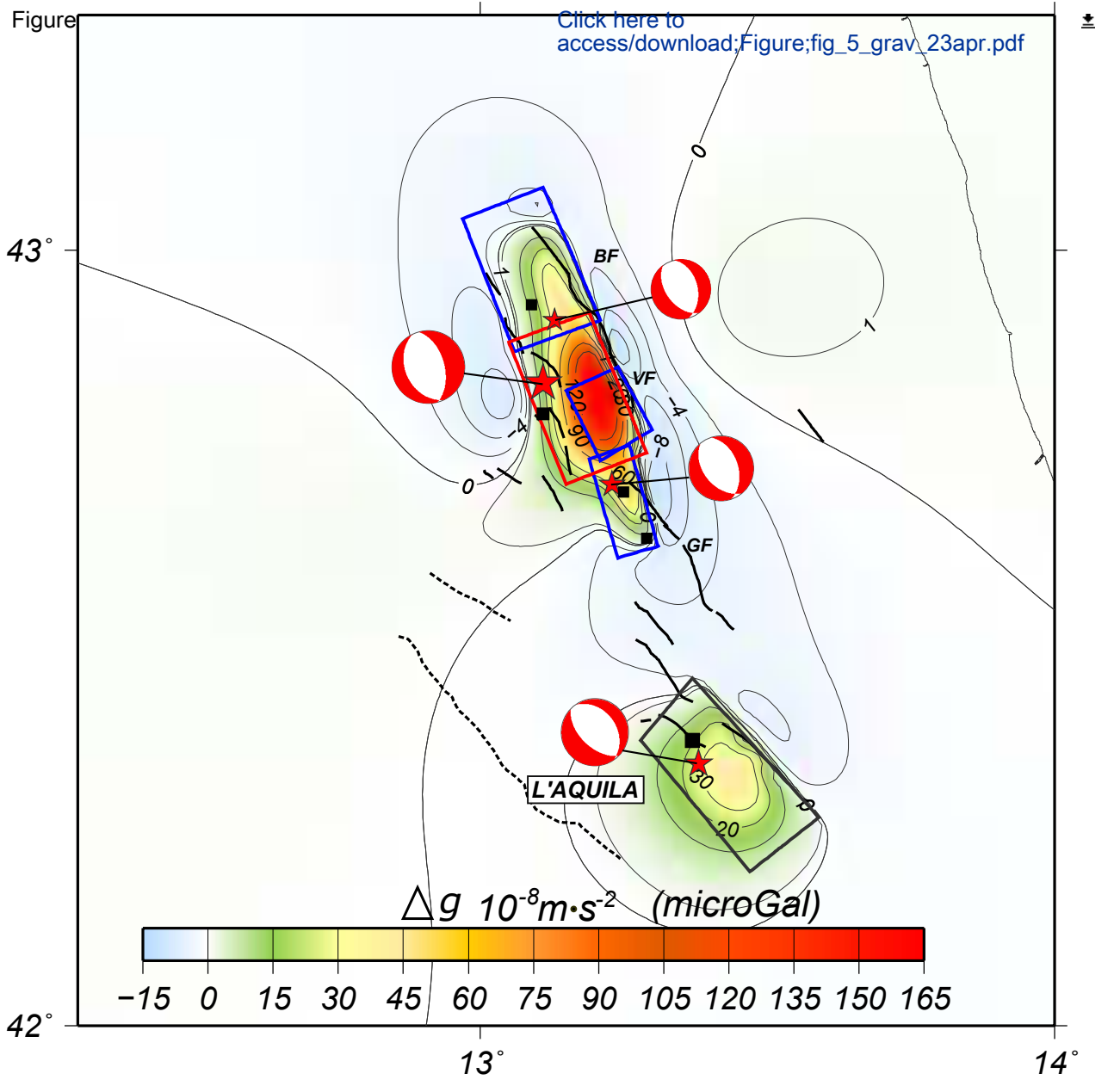

Table

| Table 1: Fault models of 2016 and 2009 mainshocks from geodetic data | | | | | | | |
|---|---|---|---|---|---|---|---|
| Seismic Event | Size (km×km) | Patches # | Peak slip (m) | Strike (deg) | Dip (deg) | Seismic Moment ($\times 10^{18}$ Nm) | Mw |
| 24 Aug. 2016 GF | 14×14 | 532 | 0.89 | 163.6 | 52 | 2.1 | 6.2 |
| 24 Aug. 2016 SVF | 10×10 | 420 | 1.40 | 168.5 | 41 | | |
| 26 Oct. 2016 BF | 20×16.5 | 94 | 0.70 | 158 | 43 | 2.0 | 6.2 |
| 30 Oct. 2016 VF | 20×19.5 | 134 | 2.22 | 158 | 43 | 8.5 | 6.6 |
| 6 Apr. 2009 | 28×20.8 | 135 | 0.77 | 140 | 50 | 3.8 | 6.3 |